communications earth & environment

Article

https://doi.org/10.1038/s43247-024-01578-2

Rapid intensification of tropical cyclones in the Gulf of Mexico is more likely during marine heatwaves

Soheil Radfar [1,2] ✉, Hamed Moftakhari [1,2] & Hamid Moradkhani [1,2]

Tropical cyclones can rapidly intensify under favorable oceanic and atmospheric conditions. This phenomenon is complex and difficult to predict, making it a serious challenge for coastal communities. A key contributing factor to the intensification process is the presence of prolonged high sea surface temperatures, also known as marine heatwaves. However, the extent to which marine heatwaves contribute to the potential of rapid intensification events is not yet fully explored. Here, we conduct a probabilistic analysis to assess how the likelihood of rapid intensification changes during marine heatwaves in the Gulf of Mexico and northwestern Caribbean Sea. Approximately 70% of hurricanes that formed between 1950 and 2022 were influenced by marine heatwaves. Notably, rapid intensification is, on average, 50% more likely during marine heatwaves. As marine heatwaves are on the increase due to climate change, our findings indicate that more frequent rapid intensification events can be expected in the warming climate.

In September 2022, Hurricane Ian rapidly intensified from a tropical storm to a Category 4 hurricane within just 2 days, as it traversed the warm waters (≥30 °C) of the Caribbean Sea, before making landfall on the Gulf coast of Florida. Within a mere 36 h, Ian underwent a staggering transformation from a tropical storm with 60 mph winds to a formidable Category 3 hurricane, boasting winds of 125 mph. Following its devastation of western Cuba, Ian experienced another rapid intensification phase over a warm region in the Gulf of Mexico. In just 8 h, the storm's maximum wind speeds surged from 120 to 155 mph, narrowly missing the Category 5 threshold by a mere 2 mph. Ian was responsible for over 150 direct and indirect deaths and $114B economic impact, making it the third costliest hurricane in United States history[1].

Variability in the intensity of tropical cyclones (TCs) prior to landfall poses a major challenge in predicting their threats to coastal communities[2]. It is estimated that intensity forecast errors are approximately 2–3 times larger for rapid changes in TC intensity than for non-rapidly intensifying events[3]. This unpredictability, coupled with a lack of appropriate preparedness, often leads to higher risk of catastrophic socio-economic damage during such events. The upward trend in the fraction of storms featuring rapid intensification amplifies this threat. According to the National Hurricane Center, rapid intensification (RI) of a TC (tropical depression, tropical storm, or hurricane) is defined as a 35 mph (~30 knots or 56 km h^{-1}) increase in maximum sustained winds over a 24 h period. Approximately 79% of major storms (Saffir–Simpson scale Categories 3–5, for which the lifetime maximum intensity is greater than 111 mph) undergo this intensification process during their life cycle[4]. A study[5] found that, the hurricane RI events with ≥70 mph increase in wind speed over a 24 h period immediately prior to landfall is expected to be 10–20 times more likely by the end of the twenty-first century compared with the late twentieth century. Practically, the frequency of RI events in a year serves as an indicator for the number of Category 4–5 hurricanes[6].

The RI of TCs is a complex phenomenon that is influenced by a variety of factors, including but not limited to high sea surface temperature (SST), low wind shear, abundant moisture and excess ocean heat content as a measure of the water temperature in the sub-surface (Fig. 1). Previous investigations have revealed that elevated SSTs are pivotal in driving the inter-annual fluctuations observed in both TC frequency and intensity. Generally, the critical temperature threshold for tropical cyclogenesis is SST > 26 °C[7,8]. Therefore, increased SSTs before and/or during a storm event have the potential to influence the evolution of a TC, causing it to undergo RI. Scientific findings have established that even moderate shifts in SST, as low as 1 °C, can increase the maximum total enthalpy (i.e., summation of sensible and latent heat fluxes) by 40% or more[9]. High SSTs persist over an extended period, better influence the water body, and increase the likelihood of RI occurrence. The requirement for a systematic framework to identify such warming events necessitates the definition of marine heatwave

[1]Center for Complex Hydrosystems Research, The University of Alabama, Tuscaloosa, AL, USA. [2]Department of Civil, Construction and Environmental Engineering, The University of Alabama, Tuscaloosa, AL, USA. ✉e-mail: sradfar@ua.edu

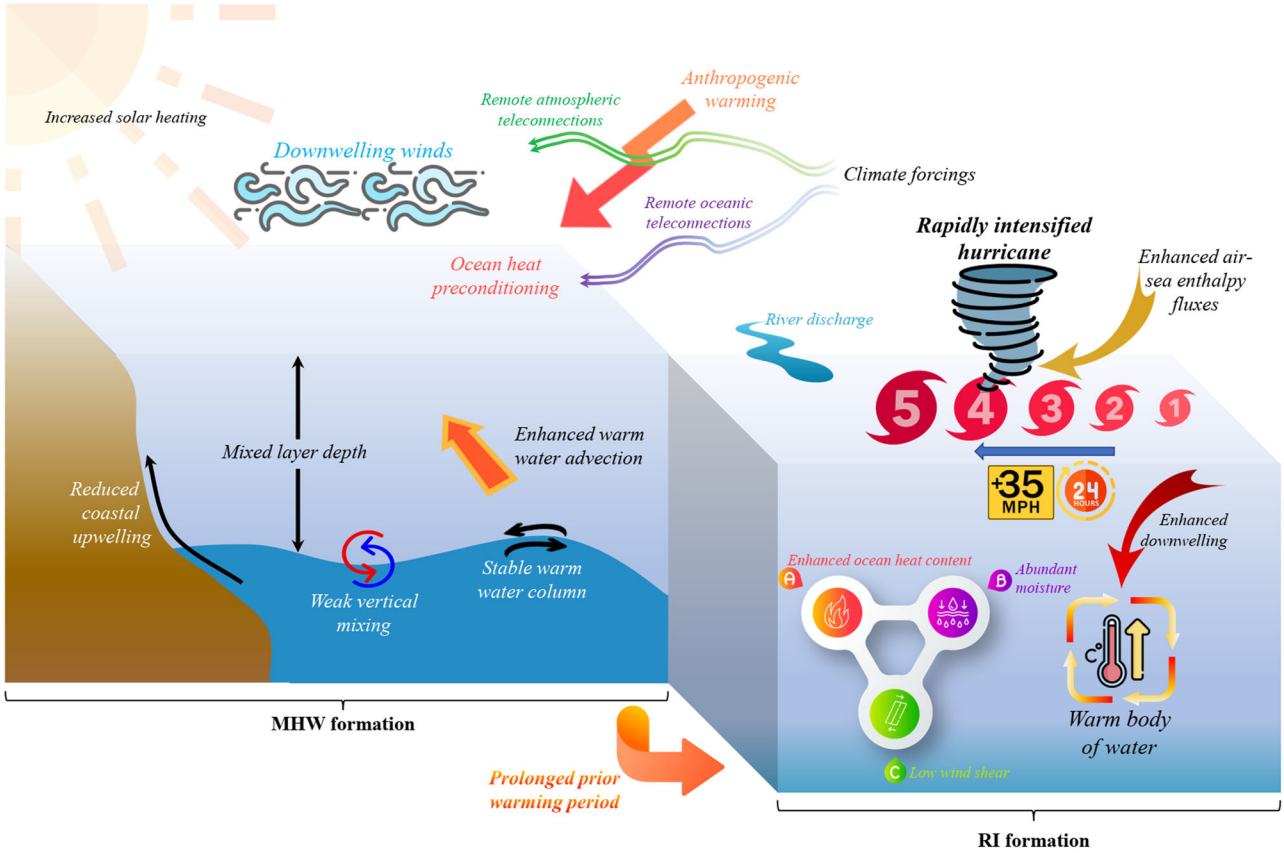

Fig. 1 | Processes involved in the formation of compounding MHW and RI events.

(MHW) as an indicator of a contiguous period of ocean water warming. MHW events are commonly characterized by at least 5 days of warm SSTs exceeding a high seasonally varying threshold above a baseline period.

The term compound weather or climate events refers to events that involve multiple climate drivers or hazards that threaten society or the environment[10]. Based on this definition, occurrence of MHWs concurrently or in close succession with RIs can be classified as a compounding event. Recent studies have highlighted the importance of MHWs as a catalyst for rapidly intensifying hurricanes[11,12]. Prolonged pre-storm warming periods due to MHWs serve as a heat source for the ocean fostering favorable conditions for the strengthening of storms. Physical evidence from TC Amphan in the Bay of Bengal[13] showcased the importance of the co-occurrence of MHW and RI events. This TC experienced higher wind speed change (55–120 knots in 24 h) compared to Fani (55–90 knots in 24 h), attributed to the coincidence of a strong MHW with this TC. These compounding effects can potentially be so strong such that they even dominate other negative atmospheric feedback to RI. As an example, for TC Amphan and Hurricane Michael[14], high vertical wind shear (VWS) could not prevent them from being intensified. Choi et al.[15] examined the impact of MHWs on TC intensity change over the western North Pacific and the Atlantic basins. They concluded that, in comparison to non-MHW TCs, the TC intensification rates for MHW TCs are about three times higher. Although this research has addressed MHW impact on TC intensity changes beyond limited and specific TC cases, further research at regional or global scales is needed to elucidate the effects of MHWs on the RI phases of TCs. A better understanding of the environmental factors affecting the RI phase is crucial for TC forecasting models[16,17]. This motivates the conduct of an in-depth MHW and RI analysis to better inform forecasting models on the magnitude of the MHW impact on this extremely difficult to predict phase of the TCs[18].

Figure 1 illustrates various atmospheric, anthropogenic, hydrologic, and oceanic processes involved in the formation of a compounding MHW-RI phenomenon. The air-sea enthalpy (heat/moisture) fluxes into the hurricane depend on both temperature difference (or sensible heat flux; SHF) and humidity difference (or latent heat flux; LHF) between the atmosphere and the upper ocean[19]. Given that surface humidity is typically estimated as a function of SST, with an assumption of near saturation, it can be inferred that higher SSTs contribute substantially to the increase of SHF and LHF toward hurricanes[14,20]. This process facilitates the upward movement of warm air (sustained convection) in the eyewall of a TC where the strongest winds are found[21,22]. The rising warm and moist air undergo condensation, which releases a large amount of latent heat. This latent heat causes the cyclone core to warm, further reducing air density and speeding up the storm[23]. Other factors like enhanced oceanic heat advection, persistent large-scale climate modes, and teleconnections as well as the ocean's anthropogenic warming not only help modulate the likelihood and severity of MHWs[24–26], but also benefit the compounding MHW-RI events by providing favorable atmospheric and oceanic conditions. The occurrence of downwelling also helps sustain increased SSTs over the ocean shelf, resulting in intensified air-sea temperature/humidity fluxes due to the enhanced SHF and LHF[22]. Downwelling favorable wind during the period of peak hurricane activity is another potential driver of strong downwelling circulation, as observed pre-Hurricane Sally[2]. Previous studies showed that subsurface ocean warming can play a key role in the generation of MHWs[27] as well as TCs[28]. Further, the rewarming of the upper ocean due to a prior TC may contribute to the favorable conditions for RI through the breakdown of stratification and enabling the warm surface layer to penetrate deeper into the ocean[2,11]. This effect was pinpointed for TCs Gordon, Hanna, and Marco preceding Hurricanes Michael, Laura, and Sally. In addition, strong salinity signals, such as those caused by river runoff, can play a crucial role in the evolution of SST, primarily through their influence on

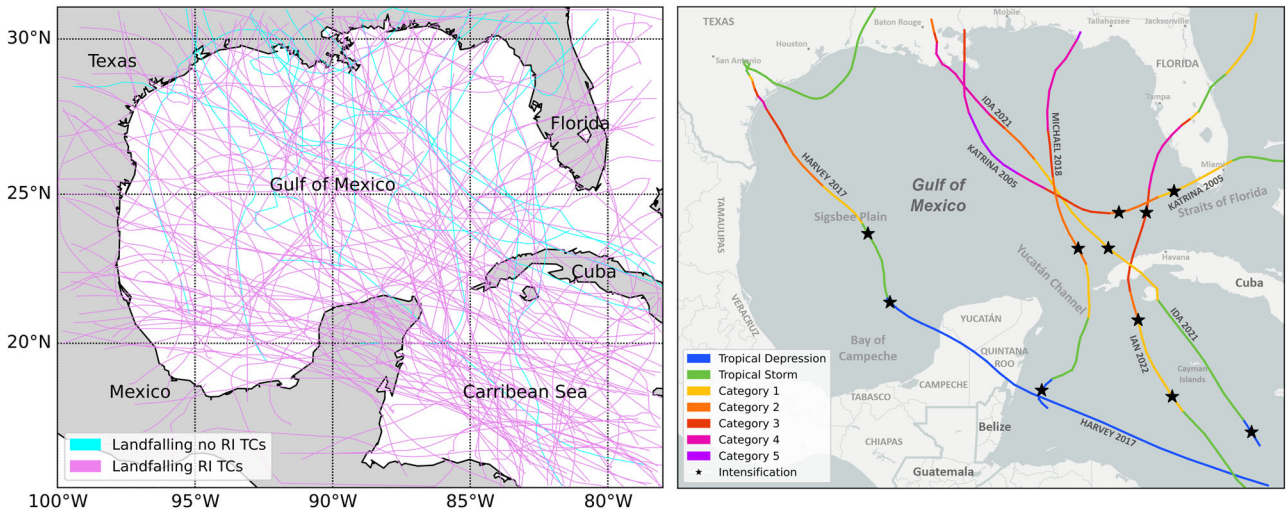

Fig. 2 | The link between landfalling and rapidly intensified TCs. Left panel: tracks of all landfalling TCs with/without RI event in the GoM and NWCS; Right panel: paths of five destructive historical hurricanes in the GoM and NWCS along with their categories and RI start locations. The track data source is IBTrACS[36].

the density structure of the upper ocean in the form of barrier layers. The function of these layers is twofold: firstly, they prevent the mixing of colder deep waters with warm pre-storm SSTs, and secondly, they restrict the cooling of the upper ocean during TCs[18,29], such as the role of Mississippi River discharge on the intensification of Hurricane Michael[14]. In addition to barrier layer thickness, reduced vertical mixing before TC passage helps sustain the MHW condition and stability of the warm column. Later, the deepening of the upper ocean mixed layer and warm ocean advection dissipate the heat, creating a larger body of warm water during the passage of TC and the intensification phase. As the primary focus of this paper is the statistical investigation of the connection between MHWs and RIs, please refer to refs. 30,31 for further details on the physical explanation of the relationship between abnormally high SST and TC RI.

The extent to which the occurrence of MHWs amplifies the occurrence of RI remains unclear. This knowledge gap coupled with the trend of warming oceans due to climate change is another motivation of the present study. In light of the expected surge in frequency and intensity of both MHWs and TCs in future warming scenarios[32,33], it becomes essential to examine the implications arising from the co-occurrence of these events and their compounding interactions. The overarching goal of this research is to determine if RIs are more likely during MHW events. To achieve this goal, we conducted a probabilistic analysis to examine the likelihood of RI occurrence in the presence of MHWs in the Gulf of Mexico (GoM) and northwestern Caribbean Sea (NWCS) and compare it to the RI probability in the absence of MHW.

Results

SST pattern across the study area

The study area is highly susceptible to hurricane activities, with approximately 68% (93 out of 136) of all hurricanes that made landfall on the continental United States between 1950 and 2022 occurring along the coastlines of this region[34]. The left panel of Fig. 2 shows the tracks of all landfalling TCs across the region, from which the paths of TCs experiencing RI are colored purple. Landfall and RI occurrences have a very strong relationship in the GoM and the NWCS. Our analysis revealed that about 70% of major landfalling TCs in the study area underwent RI at least once along their track. Among them, the RI start locations of five costly hurricanes in US history were in the study area (right panel of Fig. 2): Katrina 2005 (rank 1, $192.5B), Harvey 2017 (rank 2, $152.5B), Ian 2022 (rank 3, $114B), Ida 2021 (rank 6, $80.9B), and Michael 2018 (rank 11, $29.7B). The costs and rankings are based on a recent NOAA report on the most intense US tropical cyclones[35].

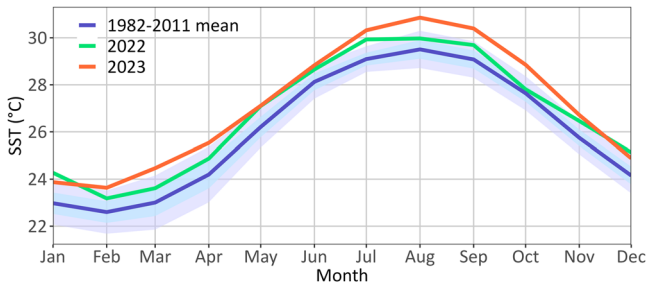

Fig. 3 | Seasonal cycle of daily SST over the GoM and the NWCS (15°N–30°N; 78°W–100°W). The climatological period is 30 years, ranging from 1982 to 2011. The envelopes show the 68% (mean ± 1σ) and 95% (mean ± 2σ) bounds. SST values in 2023 has exceeded upper historical bound and there is a significant positive anomaly compared to the last year since March. The data source is NOAA OISST V2.1[71].

Analysis of the daily SST data in the region underscores the increased likelihood of RI occurrence even more. SST values throughout the year 2023 have evidently exceeded the upper bound (i.e., +2σ) of the climatology, which is calculated based on a 30-year base period from 1982 to 2011 (Fig. 3). As per our investigation of the SST seasonal cycle in the GoM and NWCS regions during a 10-year period from 2014 to 2023, we noticed that 8 years (excluding 2014 and 2015) experienced SSTs overlapping or exceeding the mean plus one standard deviation level, in particular during hurricane season (i.e., June through November). This evidence highlights the fact that experiencing anomalous SSTs in 2023 is not simply an exception but rather becoming a norm in this region.

Probabilistic analysis of historical TC intensification events

The focal point of this study is to analyze the interaction between MHWs and hurricane RIs probabilistically. Therefore, we extracted all historical RI events (according to the standard definition of RI events by the National Hurricane Center) from the International Best Track Archive for Climate Stewardship (IBTrACS) dataset[36] (see the "Data" section in "Methods" for details). The period of our analysis spans from January 1, 1950, through December 31, 2022, with 406 unique TCs on record (excluding those marked NOT_NAMED). Based on our regional analysis, we found that within the temporal and spatial domains of our investigation, 119 unique hurricanes underwent RI, accounting for 29.3% of all recorded TCs.

In order to avoid interdependent events, we employed a 24 h minimum separation time (MST) between two successive RI events along the track of a given hurricane (see "RI definition and detection" in "Methods"). The results indicate a total of 165 RI occurrences in the GoM and NWCS. These events have been documented along the paths of 119 hurricanes, comprising 81 hurricanes that encountered a single RI event, 31 hurricanes that underwent two RI events, 6 hurricanes that experienced three RI events, and 1 hurricane that had more than three consecutive RI events. Further analysis provided in Supplementary Fig. 1 shows the intermonth distribution of RI events over the entire IBTrACS data period (1950–2022). This monthly pattern indicates that the historical RI events in the GoM and the NWCS have occurred between May to November, during the Atlantic hurricane season (June 1 to November 30). In addition, a monthly variation was observed in this pattern, with the total number of RI events throughout this timeframe surging from 12 in July to 43 (about fourfold) in August. The peak number of rapid intensifying TCs was observed in September with 53 TCs. During the Atlantic hurricane season, the areas characterized by very high ocean heat content originating from the Loop Current and its eddies, create favorable conditions for TC cyclogenesis and consequently, intensification of hurricanes[37,38].

Figure 4 depicts the spatial distribution of the probabilities of RI occurrence in the GoM and NWCS regions. Based on the calculated empirical probabilities (see Eq. (1) in "Methods") we have determined three hotspots in the GoM and NWCS areas with relatively high likelihood of RI occurrence: near the Cayman Basin in the NWCS, the Bay of Campeche (Campeche Canyon) and Yucatán Channel in the GoM. For better clarification, Supplementary Fig. 2 shows the parts of the TC tracks that experienced RI overlaid on all TC tracks' map. This figure is consistent with Fig. 4. It can be observed that a greater density of tracks and associated RI events converging over the hotspot regions. Furthermore, Supplementary Fig. 3 shows that higher maximum sustained wind speeds occur more frequently in hotspot regions due to the higher probability of RI.

Evolution of MHWs' intensity, frequency and duration over the past decades

A general understanding of long-term trends of MHW events in the GoM and the NWCS is a preliminary step to uncover the impact of MHWs on the likelihood of RI events in a changing climate. For this purpose, we implemented a MHW detection strategy to retrieve all MHWs from the ERA5 SST data based on the widely-used definition of Hobday et al.[39] (see "MHW definition and detection" in "Methods"). Two periods representing cooler (1950–1980) and warmer (1981–2022) time spans were considered to reveal spatiotemporal patterns across the study area. During the cooler era (Fig. 5a), only a few hotspots of MHWs exhibit more than 3 events per year, mostly around Cuba and Yucatán Channel. While during the warmer period (Fig. 5b), the extent of the regions was expanded to the whole of the NWCS and the southern GoM. A mean event per year of 4 days is observable on the path of the Loop Current. Previous studies have shown that the Loop Current and its eddies are the main sources of heat transport throughout the study area[40,41]. The Loop Current is a warm water current that starts in the Caribbean, flows through the Yucatán Channel into the Gulf of Mexico, and then moves clockwise. It passes by the Yucatán Peninsula, forms loop currents in the northeastern Gulf of Mexico, and eventually becomes part of the Gulf Stream as it travels through the Straits of Florida, continuing northward along the U.S. eastern coast. The current is also known as the Florida Current as it flows through the Straits of Florida. Figure 5c, d demonstrates that the mean of i_max_rel, which represents the maximum intensity relative to the SST threshold[39], is in the range of 0.1 to 1.0 °C per year, with a positive shift toward higher intensities during warming climate. Also, over the GoM, although we see a lower number of MHW events, with more intense i_max_rel, alarming reaching higher SST levels. Overall, the Texas-Louisiana Shelf and West Florida Shelf show higher maximum intensity levels during both cooler and warmer periods. Pattern of mean duration of MHW events (Fig. 5e, f) the indicates that during the warmer period, MHW events last almost anywhere longer than the cooler period. Climate change has led to a substantial increase in the average duration of MHWs within the study area, rising from 36.5 to 49.5 days per year. It is apparent that the NWCS and along the Loop Current path at the Yucatán Channel and Straits of Florida experience notably prolonged MHWs. The southwestern GoM has also experienced rather prolonged MHWs due to the Yucatán Current that brings warm water from the Caribbean Sea to the Western GoM. Further analysis of the relationship between i_max_rel and duration in Fig. 6 reveals that longer events tend to occur with lower i_max_rel at higher maximum intensities, and vice versa. This finding is in full agreement with Fig. 5c–f. The results indicate that short-duration anomalies dominate in both periods, but there is a slight increase in longer events in the recent period. Moreover, the duration density plot shows that events with short-duration anomalies experience a sharp decline in frequency as their duration increases. Broader spread of higher intensity values reflects an apparent shift toward more intense SST anomalies in the warmer period. The density plots along the i_max_rel peak near zero, indicating that most SST anomalies were close to the MHW detection threshold level. A further observation in Fig. 6 is that all MHWs have an SST above 26 °C, which is the minimum temperature that favors TC formation. Accordingly, in our study domain, PC80 threshold captures more severe events with an impact on TC strengthening.

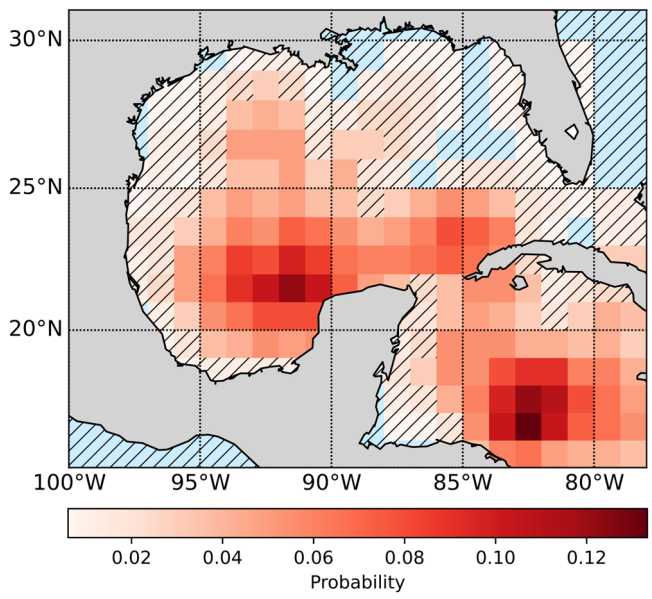

Fig. 4 | The probability of RI occurrence in the GoM and NWCS regions. The light blue grids demonstrate the locations with insufficient historical information. Hatches represent the grids where the estimated probability is not statistically significant (p_value > 0.1).

Contribution of MHWs in enhancing the likelihood of RI events

The main question revolves around the extent to which the occurrence of MHWs, within a reasonable temporal and spatial distance, impacts the likelihood of RI events. To address this question and establish a quantitative framework, we implement conditional probability analysis. Hence, we calculate $P(RI|MHW)$ (see Eq. (2) in "Methods"), which represents the probability of RI occurrence given a MHW pre-condition. An important step toward the quantitative analysis of MHW impacts on RI events is to find out those MHWs that occurred within a reasonable spatial and temporal distance to the historical RI events. For this purpose, this study leverages a double-threshold approach (see "Relevant" section in "Methods" for further details) to filter the MHWs that influenced the RI of historical hurricanes. Employing the double-threshold methodology, we identified all MHWs that have occurred within 10 days and 125 miles of the beginning of RI events (hereinafter called impact area). The pool of influential MHWs on RI events encompasses 5242 events. These MHW events were identified

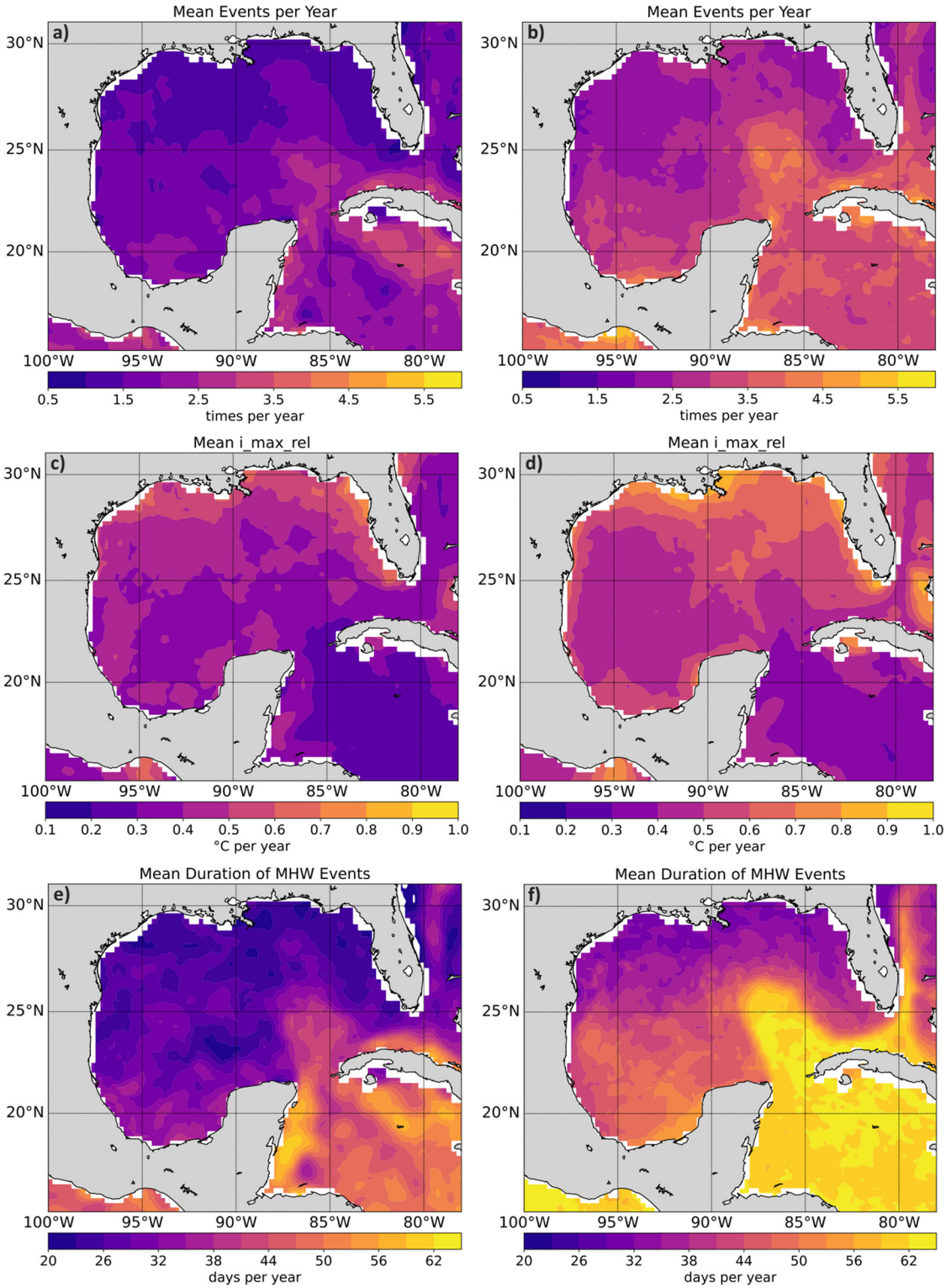

Fig. 5 | Comprehensive statistical analysis of historical MHWs for two periods across the GoM and NWCS. Left panel shows the cooler period from 1950 to 1980 and right panel shows the warmer period from 1981 to 2022. **a**, **b** Mean number of events; **c**, **d** mean of maximum intensity relative to PC80 threshold; **e**, **f** mean duration of events.

based on a set of criteria, including a minimum separation time of 24 h for RI events, an SST threshold percentile (PC80), a minimum duration of 5 days, and a maximum gap of 2 days for detecting MHWs. Our analysis showed that 75 unique TCs (≈ 69.44% of all TCs) had at least a MHW within their impact area. Figure 7 shows that MHWs have significant impacts on RI events in nearly all grids of the NWCS, as well as the southern and northwestern GoM. This also accords with our evidence shown in Fig. 5. It is expected that regions with a higher mean number of events (Fig. 5a, b) and longer mean durations (Fig. 5e, f) will see a stronger contribution of MHWs to historically rapidly intensified TCs. This is because more frequent and temporally extended MHWs provide more likely TC exposure to a persistent heat source. Furthermore, the spatial pattern of RI occurrence in Fig. 4 is consistent with Fig. 7, highlighting the fact that the presence of MHWs is influential in increasing the RI probability over the hotspot locations.

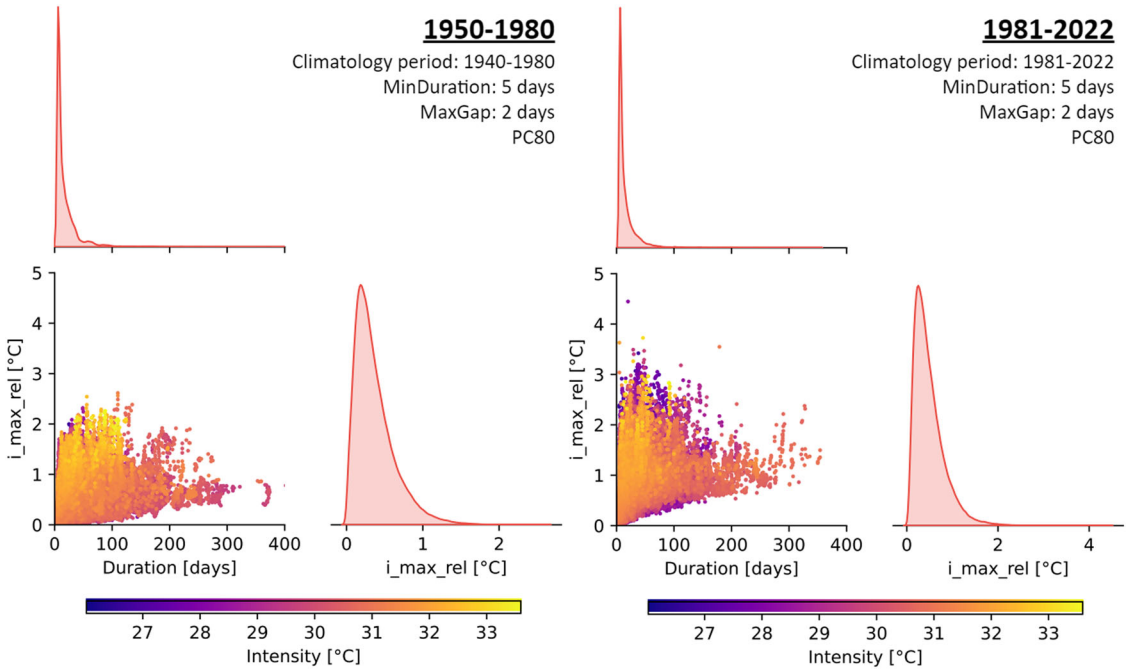

Fig. 6 | Pair plots of maximum intensity relative to the SST threshold [°C] and duration [days] across the GoM and NWCS. Left panel shows the cooler period (1950–1980) and the right panel shows warmer period (1981–2022). Each pair color indicates its absolute maximum intensity (or SST).

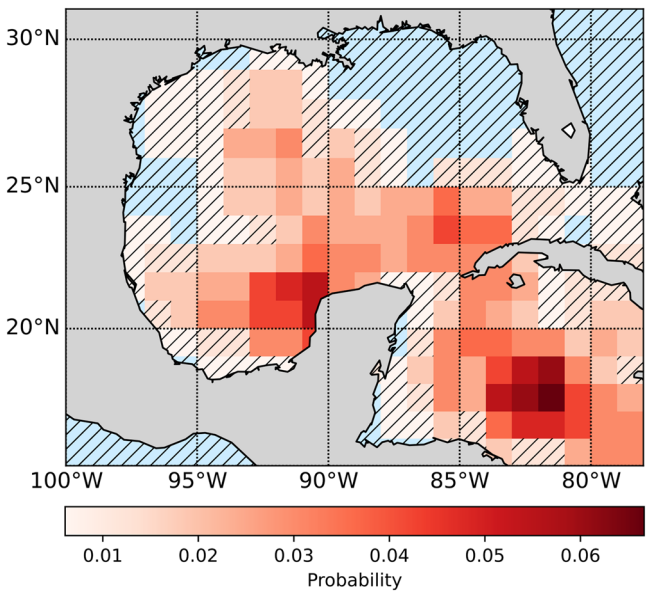

Fig. 7 | Conditional probabilities of RI occurrence given MHW occurrence. Adopted scenario: MST = 24 h, PC80, Minimum duration = 5 days, Maximum gap = 2 days. Light blue grids show the locations with insufficient historical information.

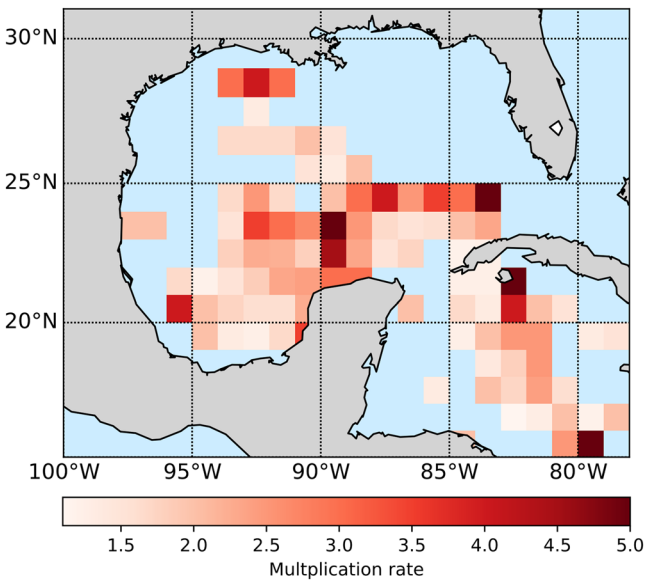

Fig. 8 | Regions with increased RI likelihood due to MHWs. The gridded rates represent the ratios between the conditional probabilities of RI occurrence in the presence of MHWs to the conditional probabilities in their absence. Adopted scenario: MST = 24 h, PC80, Minimum duration = 5 days, Maximum gap = 2 days. The light blue grids demonstrate the locations with insufficient historical information.

An important question that this study aims to answer is: What is the extent to which the occurrence of RI events increases in the presence of MHWs compared to their absence, i.e., $P(RI|\overline{MHW})$? For this purpose, the gridded multiplication rates (see Eq. (3) in "Methods") have been calculated and represented in Fig. 8. Consistent with our physical understanding, the multiplication rate is substantial in regions with high $P(RI|MHW)$. The multiplication rate equal to 1 signifies that the likelihood of RI events is the same regardless of whether MHWs are present or not. In accordance with Figs. 4 and 7, in the southwestern GoM, near the Yucatán Channel, and the Yucatán Basin in the NWCS demonstrate the highest magnified likelihood in the presence of MHWs. We also see considerable multiplication rates near the Texas-Louisiana Shelf that showed significant i_max_rel according to Fig. 5c, d. Interestingly, the results suggest that the interaction of MHWs and RIs can amplify the likelihood of experiencing rapidly intensified TCs up to 5-fold (on-average 1.5-fold) over the identified hotspot regions. These findings on the prevalence of significant multiplication rates emphasize the importance of enhancing our understanding of the potential co-occurrences of MHW and RI events, as well as the compounding events that stem from their interactions.

Discussion

This study unveils an amplification pattern of the likelihood of RI in the presence of MHWs. We conducted a comprehensive analysis of the IBTrACS dataset spanning 1950–2022 across the GoM and NWCS regions. The results indicated that 67% of TCs with lifetime maximum intensity exceeding 111 mph (indicator of major storms in Saffir–Simpson Hurricane Wind Scale) have experienced at least one RI event before making landfall. This rate is considerable for a distinct geographical domain that may not necessarily encompass the complete track of all TCs during their lifetime. An MST of 24 h was considered to ensure the assumption of independence for RI events.

In the present study, MHWs were characterized based on the setting proposed by Hobday et al.[39], which is a minimum duration of 5 days and maximum gap of 2 days. In any case, it should be noted that this definition was based mostly on atmospheric heatwaves and has been extensively applied in studies of marine ecosystems (see refs. 42,43 among others). The extremely high thresholds applicable to heatwave impacts on marine ecosystems may not apply to the RI of TCs. A persistent ocean warming event with less strict settings can potentially provide sufficient conditions for rapid changes in maximum sustained wind speeds. Physical evidence also supports such adjustments. For example, the percentile-based definition raises concerns, particularly regarding the discontinuities in exceedance rates observed at the start and end of the baseline period. Zhang et al.[44] using Monte Carlo simulation observed such discontinuities as a sudden increase in the temperature exceedance rate at the beginning and the end of the base period. In order to encompass MHWs with lower frequencies and weaker cumulative intensities, Zhang et al.[45] introduced two major modifications to the definition. A modification they made was to calculate the climatological mean from the original data without applying any smoothing filters, since this step would artificially increase the intensity and prolong the duration of MHW events. The second adjustment involves incorporating the calculation of MHWs on 29 February during leap years. This allows reliable examination of daily MHW variations both in regular and leap years. Such deviations from the widely-used definition by Hobday et al.[39] are also supported by the observations of Dzwonkowski et al.[2]. They compared the evolution of the depth-average temperature from 2020 to climatological conditions, in the case of Hurricane Sally. It showed that while this increase in depth-average temperature did not reach the threshold for a MHW, the temperatures were well above the values that have been statistically associated with rapidly intensifying TCs. These observations led us to use the PC80 threshold instead of PC90, which is a widely used SST threshold level within the context of MHWs. This helped our framework capture other frequent but less extreme ocean warming events that were highlighted in the aforementioned studies.

Employing our proposed double-threshold methodology to identify influential MHWs for the formation of RI events, we found that approximately 70% of TCs experienced at least one MHW within their impact area. Our findings suggest that the contribution of MHWs on up to 5-fold amplification of the likelihood of RI events is prevalent in the NWCS and the southern GoM. These hotspots overlay the regions with higher mean events and duration per year due to higher exposure to heat source, as evidenced by the spatial patterns provided in Fig. 5. A large part of this contribution can be attributed to the enhanced Tropical Cyclone Heat Potential (TCHP), which serves as a measure of the subsurface heat accumulation. TCHP (see Eq. (4)) reflects stored upper ocean thermal energy and has a strong connection to pre-storm SST conditions[14,46]. The enhanced TCHP prevents the SST cooling triggered by TCs. This enables the persistence of warm ocean temperatures necessary for sustaining MHW events and fostering RI[13]. It is worth mentioning that ocean heat content has substantially increased since the mid-twentieth century both globally[47–49] and in the North Atlantic[50,51]. Therefore, TCHP is expected to become even more readily available to fuel TCs. The data presented in Table 1 shows that the locations of RIs for four costly TCs (Harvey 2017, Michael 2018, Ida 2021, Ian 2022) were characterized by a TCHP in the range 83–184 kJ cm^{-2}. These values can be considered remarkable anomalies as TCs are prone to strengthening in areas where the TCHP exceeds 50 kJ cm^{-2} in the Atlantic Ocean[46]. TCHP is calculated based on the depth of 26 °C isotherm (D26). This temperature is a reasonable proxy for the potential for TC intensification, and D26 indicates the extent of penetration into deep ocean depths. A deeper D26 can provide a larger heat reservoir for the TC to draw upon, possibly contributing to a higher RI likelihood. In agreement with Fig. 7, the TCs that experienced RI in the CS are associated with higher TCHP values as well as deeper mixed layer depth (MLD) and D26. Deeper MLD indicates that the well-mixed warm ocean surface layer extends further down. This means that the TC has to churn through a greater volume of warm water before it reaches cooler layers, which could otherwise weaken the storm. For each event, the characteristics of the MHW with minimum spatial gap are also summarized in Table 1. As can be seen, events with lower end gaps and distances to the beginning of RI often correspond to higher TCHP values. Notably, the RI of these TCs appears to be mainly influenced by the MHWs with slight deviation from the threshold level and maximum intensities (i_max) above 30 °C. It is due to the fact that RI occurrence rate is multiplied in this region at SSTs above 29 °C[52]. A similar finding was found in Fig. 6, where long-lasting events with high intensities were associated with lower i_max_rel both during cooler and warmer periods.

As discussed above, apart from high TCHP, other factors like low wind shear and abundant moisture are also have crucial roles in initiating RI events. Figure 9 illustrates the spatial distributions of mean TCHP, mean VWS, and mean LHF as a representative of moisture conditions. Figure 9a shows that there is a good agreement between the spatial pattern of TCHP and Fig. 4, suggesting that the MHWs have subsurface structure and are not limited to surface SSTs only. Essentially, this subsurface warm body of water represents available oceanic, which can further fuel TCs. Recently, Ray et al.[53] highlighted the role of extending warming from surface MHWs to the subsurface in transforming Cyclone Yaas (2021) from a tropical depression to a very severe cyclonic storm. Apart from TCHP, wind shear is another crucial factor. VWS values of less than 10 m s^{-1}, especially around 5 m s^{-1}, favor rapid intensification[54,55]. The spatial pattern of Fig. 9b shows that wind shear is very likely to prevent TC intensification in many regions of the GoM and the NWCS. This indicates that the favorable conditions due to the presence of MHWs is a necessary but not a sufficient condition for RI formation, and this is one of the reasons that the gridded probabilities in Fig. 7 are about half as large as in Fig. 4. LHF is another crucial factor in the net surface energy flux during this process[56]. Its role outweighs SHF, which is related to the temperate difference between the ocean and atmosphere[57]. Figure 9c demonstrates that on average, the northern parts of the GoM, north of Cuba and southeast of the study area in the NWCS have less conducive conditions in terms of LHF for RI formation. The synchrony of the aforementioned influential factors is the ideal case for RI initiation, which is apparent is not plausible in every time span or location. For example, although the observation of relatively high TCHP values throughout the NWCS is a positive driver of RI, the LHF and VWS have the potential to suppress this phenomenon in some regions. This could be potentially one of the reasons that not necessarily all the regions with high TCHP exhibit high probability of RI occurrence. It is noteworthy that these diagrams are merely spatial patterns suitable for providing a general overview of the underlying physics before the onset of historical RIs. The co-varying relationships between these variables and other possibly influential environmental parameters such as salinity[18] should be examined for each event individually to have better insights into the local variations that occur before each RI event.

Overall, the presented quantification framework contributes to better understanding how MHWs influence RI events, and the compounding events that result from their interaction. This research provides a basis to facilitate proactive measures against highly intense TCs, thereby improving resilience and preparedness efforts to mitigate the potential catastrophic consequences. While high probabilities of encountering prolonged periods of high SST could potentially facilitate the occurrence of RI events, it is important to acknowledge that MHWs are just one of several preconditioning factors contributing to the RI of TCs. In order for a storm to

Table 1 | Summary of oceanic and thermal structure data related to RI points of Hurricanes Harvey (2017), Michael (2018), Ida (2021), and Ian (2022)

RI event information	Event number	1	2	3	4	5	6	7
	Hurricane name	Ian	Ian	Ian	Ida	Michael	Harvey	Harvey
	Basin	CS	CS	GoM	CS	GoM	GoM	GoM
	RI start latitude	15.0	18.7	22.6	17.0	23.2	21.4	23.7
	RI start longitude	−79.4	−82.4	−83.6	−79.2	−85.5	−92.3	−93.1
	RI date	9/25/2022	9/26/2022	9/27/2022	8/26/2021	10/9/2018	8/23/2017	8/24/2017
Ocean variables	TCHP (kJ cm^{-2})	97.3	183.8	162.1	131.3	90.6	83.1	86.1
	MLD (m)	36.1	60.9	57.2	76.9	39.3	39.6	32.3
	D26 (m)	71.4	141.9	127.4	147.3	88.1	64.7	58.5
MHW event with minimum spatial	Distance (km)	16.1	11.9	11.1	47.0	103.0	152.5	11.6
	i_max_rel (°C)	0.61	0.54	1.18	0.39	0.10	0.33	0.31
	i_max (°C)	30.0	30.4	30.9	29.6	29.6	29.7	30.5
	Duration (days)	10	8	43	13	5	5	30
	Start gap (days)[a]	−19	−7	−42	−17	−11	−10	−36
	Peak gap (days)[a]	−16	−2	−2	−11	−11	−8	−35
	End gap (days)[a]	−10	0	0	−5	−7	−6	−7

The columns have been color-coded based on their cell values (dark red: higher value; light red: lower value).
[a]Start, peak and end gaps indicate the time gaps (days) between the start, peak and end of the MHW event and the start of the RI event.

strengthen, the combination of favorable large-scale atmospheric conditions and underlying oceanic conditions must align as well. A brief discussion of the physical drivers for compound RI and MHW events has been presented so far. However, a profound understanding of these compounding events generally demands case-by-case investigation of TCHP, downwelling conditions, mixed layer depth, barrier layers, preheating and rewarming behavior of the ocean water body, such as those carried out by Dzwonkowski et al.[11] and Le Hénaff et al.[14] for Hurricane Michael, or Dzwonkowski et al.[2,58] for Hurricane Sally. Another crucial mechanism in this region is El Niño. This climate pattern causes stronger wind shear over the GoM and the NWCS, and suppresses hurricane activity[59]. It is noteworthy that hurricane activity in 2023 was above normal despite the prevailing El Niño conditions during the 2023 Atlantic hurricane season, as VWS due to the El Niño effect was below normal in most parts of this region from August to October[60]. This is likely due to the extra-warm Atlantic waters, which favored anomalous upward motion over the region, counteracting the El Niño effect. However, this effect is not yet fully understood[60]. Further study is needed to uncover the interconnections between El Niño, MHWs, and RI.

A limitation of this study is that our findings are based on historical events. This opens up opportunities for improvement. To bolster the statistical significance of the findings and address the data scarcity issue for compound RI-MHW impact analysis, future work could incorporate physically-based synthetic TC scenarios, particularly for future projections. For instance, simulating synthetic TC tracks using wind statistical estimation tool based on Markov chains[61,62] or implementing a statistical-deterministic TC model to generate large numbers of synthetic TCs under historical and future projected climate conditions[63,64]. Machine learning algorithms, in particular LSTM (stands for long short-term memory networks), can also be leveraged to predict RI events (refer to refs. 65,66 for further details). Recently, Jacox et al.[67] developed a tool to forecast MHWs up to a year ahead using a large multimodel ensemble of global climate forecasts. It is evident that the application of the presented methodology for

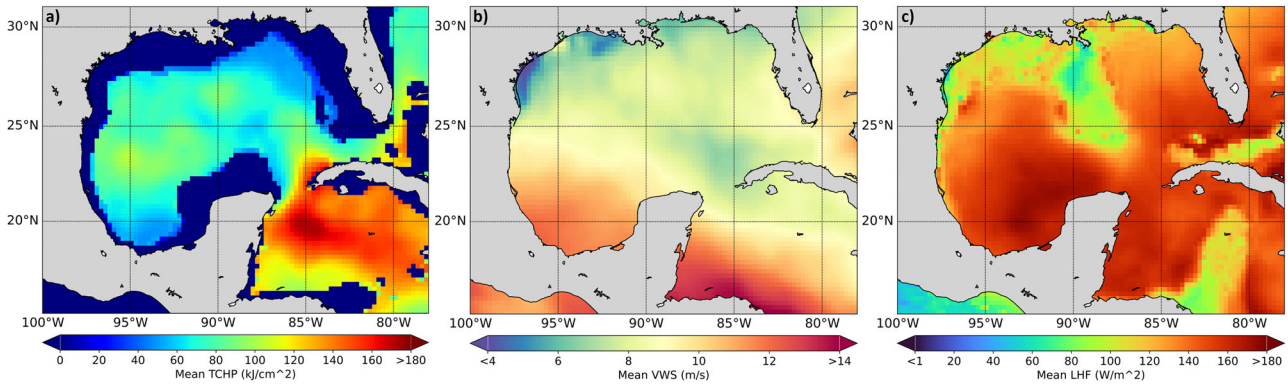

Fig. 9 | Wind shear, ocean thermal and humidity conditions during RI events. Spatial distribution of (**a**) mean TCHP, (**b**) mean VWS, and (**c**) mean absolute LHF across the GoM and the NWCS. Values are averaged over a 10-day period before the onset of RI events occurred between 2013 and 2022. The dark blue (negative) values in the TCHP plot denotes the grids without data.

the quantification of the compounding probabilities of MHW and RI events under enriched datasets of historical and future climates would be even more informative. As a concluding remark, it should be mentioned that the annual SSTs in the GoM and the NWCS are expected to increase by 2.2–2.8 °C by the end of the twenty-first century under RCP8.5 (with the rate of 0.4–0.5 °C per decade)[68]. Continued ocean warming in this region, as exemplified by the impacts of Hurricane Ian[1], can lead to far-reaching consequences. This is not just an exception specific to the study area. From a global perspective, there has been a more than 50% rise in the reported annual number of MHW days throughout the past century[69]. The spatial distributions of changes in annual MHW days, frequency, and cumulative intensity are expected to exhibit a 4-fold increase under a moderate greenhouse gas emission scenario (i.e., SSP245)[70]. The increasing frequency and intensity of MHWs in the world's oceans act as a supercharger for TCs globally (see Fig. 1), increasing the risk that they could experience RI.

Methods

Data

The IBTrACS[36] (or, the International Best Track Archive for Climate Stewardship) used for analyzing hurricane data in the implemented analyses. IBTrACS integrates TC data from multiple global agencies to create a unified, publicly available, best-track dataset that enables inter-agency comparisons. This dataset spans from the 1840s to the present and provides three-hourly information. The other component of current probabilistic analysis is SST data for MHW characterization. There are also several SST datasets available for MHW detection. While the NOAA Optimum Interpolated SST (OISST) version 2.1[71] is the commonly used dataset in heatwave studies[11,39], the European Centre for Medium-range Weather Forecast (ECMWF) Re-Analysis 5 (or, ERA5) dataset[72] provides a much longer and more consistent record of SST data with superior temporal resolution (hourly versus daily data) compared to other alternatives. The significance of having a long-term record lies in the fact that our analysis spans hurricanes from 1950 to 2022, necessitating a historical baseline period that adequately covers this timeframe. ERA5 SST data has been proven to be of high quality and adequate throughout the GoM and the NWCS[73]. So, we used it to provide a robust and comprehensive understanding of the impact of MHWs on TC RI in the study region. The MHW analysis was performed by obtaining daily-averaged SST data from the ERA5 SST dataset from January 1, 1940 to December 31, 2022.

RI definition and detection

Based on the definition proposed by the National Hurricane Center, a RI event is characterized by a minimum 35 mph increase in maximum sustained wind speeds over a 24 h period[52]. To extract RI events, we analyze IBTrACS data over the study region by identifying TC RI events that meet the specified criteria from January 1, 1950 to December 31, 2022. We found a total of 738 RI events. Given that RI events are determined based on the 3-hourly best track intensity, it is conceivable that there might be overlap between sequential RI events within a 24 h timeframe. To alleviate this issue and ensure reliable estimation of underlying trends and prevent misinterpretation, a declustering scheme by utilizing an MST was considered. This time interval must be longer than the typical duration of the physical processes generating the events and not too long, to discard independent events and lose valuable information[74]. Kossin et al.[75] showed that events separated by at least 18 h can be considered independent. Since RI events can span for 24 h, an MST equal to 24-h was deemed sufficient to ensure independent events and avoid overlapping RI events. From a probabilistic viewpoint, we aim at calculating the gridded probability of RI occurrence, i.e., $P_{RI}(i,j)$, as presented in Eq. (1):

$$P_{RI}(i,j) = \frac{N_{RI}(i,j)}{N_{RI}(T)} \tag{1}$$

where i and j are latitude and longitude indices each 1°× 1°computational grid of the area of interest and $N_{RI}(i,j)$ denotes the count of RI occurrences in the grid cell with indices i and j, $N_{RI}(T)$ is the total number of RI events across the whole domain in the time period of 1950 to 2022. In our probabilistic analysis, the criterion to identify statistically significant grids is to have p value ≤ 0.1, which is equivalent to the confidence interval of 90%. Consequently, hatched grids represent locations with a statistically insignificant probability estimate. In other words, considering the confidence level of 90%, the observed data in these areas do not provide strong enough evidence to confidently support a significant or meaningful calculation of P_{RI}.

MHW definition and detection

MHWs are defined as discrete (or continuous), prolonged, anomalously high SST events that last from several days to several months or even longer, ranging from several miles to several thousand miles in size[25,69]. Although several MHW definitions have been proposed, Hobday et al.'s definition[39] has been widely adopted. They defined MHWs as ocean warming events with SSTs surpassing a seasonally evolving threshold for at least five consecutive days. Using seasonally varying thresholds, rather than a fixed mean annual threshold, this definition enables the detection of MHWs throughout the year, such as distinguishing summer and winter MHWs[12,76]. The MHW detection is implemented with an R package, called "heatwaveR"[77], based on the ERA5 SST dataset. In this process, MHWs are identified at each latitude and longitude as warming events where daily-averaged SSTs exceed the seasonally varying PC80 values for a minimum of five consecutive days. In our analysis, if there is a gap of less than 3 days between two events, they are treated as a single continuous MHW event. This choice is justified by the requirement that a warm event needs to last at least 5 days to be classified as

an MHW, and the upper ocean temperature responds to changes in surface heat flux on relatively short time scales of hours to a day[12]. The uncertainty of MHW identification mainly stems from SST products. Therefore, the definition of MHWs here is based on the seasonally evolving threshold to identify anomalously warming events[45]. Moreover, a moving 11-day window size was chosen for the threshold calculation since the minimum duration of a MHW is 5 days and this also ensures sample sizes are sufficient for the estimation of means and percentiles[12,76]. Also, the climatology and threshold were smoothed by applying a 31-day moving average. This smoothing technique helps deal with the high-frequency noise from climatology and threshold calculations[26,76]. Selection of the baseline period is also critical for climatology calculation and greatly impacts the entire process. While Hobday et al.[39] suggested a minimum of 30 years, it is recommended to opt for a longer duration. This is to mitigate the influence of localized decadal trends on MHW frequency. Longer baselines could introduce bias as the data coverage might be uneven. For instance, cells with data available only in recent decades due to global warming, would exhibit higher temperatures, leading to higher MHW thresholds. It should also be noted that the potential intensity of tropical cyclones depends on the relative SST, that is, the local SST minus its tropical mean SST[78,79]. Therefore, it could be misleading to use a single relatively long baseline period to detect the incidence of MHWs over several decades (>50 years) with various stages of intense warming. For these reasons, von Kietzell et al.[80] used 50-year baseline to reflect a subjective balance between the two considerations. Similarly, we deployed two climatological periods of 1940 to 1980 (41 years) and 1981 to 2022 (42 years) as our baseline periods to estimate the percentile thresholds and mean climatological SST. The extent to which MHWs are related to mean background warming or variance in non-seasonal temperatures may heavily influence this impact[76].

Double-threshold approach: filtering influential MHWs

The identification of influential MHW events in the present study relies on two key factors: the time window relative to the beginning date of RI, and the distance from the RI start location. To ensure that these criteria are met, we developed a double-threshold approach to initially identify MHWs that exhibit close spatial and temporal connections with historical RI events. It should be highlighted that there are other factors such as length scales of SST anomalies and the translation direction and speed of the TC that contribute to the onset and magnitude of RI that were not included in the present analysis[81].

Our approach is established upon two temporal and spatial thresholds that represent these factors. The precise time window during which a hurricane can be affected by an ocean warming event is still an area of active research and may vary depending on the circumstances. Some studies[14,82] focused on the first few days after the MHW event ends to address the strongest impact of an ocean warming event on RI event, while others[2,11] suggest that the impact may continue for several weeks or more and a sequence of vertical mixing, horizontal advection, upwelling and surface heat flux can contribute to favorable shelf conditions for RIs. In the present study, the temporal threshold is defined such that the time span of a MHW event must fall within 10 days of the beginning date of RI. This choice is consistent with the sliding window used to calculate climatology and threshold percentile for defining MHWs[39,77]. It is noteworthy that Dzwonkowski et al.[11] used a similar timeframe to study the link between MHWs and RI for Hurricane Michael (2018) in the eastern GoM.

For the spatial threshold, we only include MHWs that are located within 125 miles (≈ 200 km) of the start location of RI event. This is inspired by the findings that in addition to the effective radius of the hurricanes (which is 7–8 times the radius of the maximum wind speed or approximately 100 km from the eye out[83]), the air-sea enthalpy (heat/moisture) fluxes in the outer core to the eyewall of the hurricane play a vital role in maintaining and enhancing the moisture in the boundary layer to support RI[14,84]. The size of the outer core can vary depending on several factors, including environmental humidity, vortex structure, sea surface temperature, and latitude and longitude[85]. Calculations in the study area showed that the mean radius of maximum wind (RMW) is 41.4 km and the average R34 is 109.7 km. According to Wang and Xu[86], an entropy flux within 2–2.5 RMW (≈R34) plays a crucial role in balancing the high dissipation occurring near the inner-core region and contributes to their intensification. Given that thermal displacement during MHWs can spatially extend from tens to thousands of kilometers[87,88], considering approximately twice R34 as the spatial threshold for compounding MHW-RI analysis is deemed meaningful. This is consistent with the definition of Weatherford and Gray[89] for outer core radius. They defined it as the region between radii of 1° and 2.5° latitudes. Our spatial extent is more restrictive than those used in the literature, including 500 km by Mawren et al.[12] and 300 km by Rathore et al.[13].

Mathematical representation of the probabilistic analysis

To calculate the probability of RI given a pre-existed MHW in grid (i,j), during which the wind speed change (ΔW_s) of at least 35 mph in 24 h (Δt_{ri}) occurs, and for an MHW_m the temporal and spatial distance to RI_k is maximum 10 days (Δt_{mhw}) and 125 miles (d_{mhw}), we use Eq. (2). Hence, the gridded conditional probability of RI occurrence given the MHW occurrence, is used to quantify the impact of MHW presence on RI events as follows:

$$\begin{aligned} &P(RI|MHW)_{ij} \\ &\quad = P\left(RI_k \cap MHW_m \,|\, \Delta W_s \geq 35\ \text{mph}, \Delta t_{ri} \leq 24\text{hrs}, \Delta t_{mhw} \leq 10\text{days}, d_{mhw} \leq 125\text{miles}\right)_{ij} \\ &\quad = \frac{\sum_{m=1}^{M_{ij}} \sum_{k=1}^{N_{tc_{ij}}} \left(N_{tc_{ij}|\Delta W_s \geq 35\text{mph}, \Delta t_{ri} \leq 24\text{hrs}} \cap N_{mhw_m|\Delta t_{mhw} \leq 10\text{days}, d_{mhw} \leq 125\text{miles}}\right)}{N_{RI}(T)} \end{aligned} \tag{2}$$

where $P(RI \cap |MHW)$ represents the probability of coincidence of RI and MHW events within each 1°× 1° computational grid, fulfilling the aforementioned requirements. Same as Eq. (1), $N_{RI}(T)$ denotes the total number of TCs across the whole study area, and M_{ij} is the total number of MHWs that in that occurred grid. In the numerator, the inner sigma loops over each TC of the grid to identify those that meet the criteria for RI occurrence. Then, for each RI event, it searches for the number of MHWs that fall within the impact area based on the double-threshold approach. Accordingly, each count of compound RI and MHW events accounts for one co-occurrence and adds 1 to the numerator of Eq. (2). A similar methodology has been used recently to compute the conditional joint probability of compound drought and heatwave event by Tripathy et al.[90].

Finally, the most informative parameter in identifying the amplifying impact of MHWs' presence is the multiplication rate. This can be defined as the ratio between the conditional probabilities of RI occurrence in the presence of MHWs, i.e., $P(RI|MHW)$, and the conditional probabilities in their absence, i.e., $P\left(RI\middle|\overline{MHW}\right)$:

$$\text{Multiplication rate} = \frac{P(RI|MHW)}{P(RI|\overline{MHW})} \tag{3}$$

The above ratio denotes the actual impact of MHW presence on amplifying the likelihood of hurricane RI events. This assists in the pinpointing and analysis of the contribution of MHWs to strengthening the TCs.

To further elaborate on the oceanic and meteorological conditions before the beginning of RI events, we acquired TCHP, D26, and MLD from NOAA's operational satellite ocean heat content product that has a grid resolution of 0.25° with temporal extent from Aug 27, 2012 onwards[91]. The MLD is defined as the depth where the temperature deviates from the SST by 0.5°C. In this dataset, TCHP is computed from the ocean surface to the depth of the 26 °C isotherm (D26) using the following equation:

$$\text{TCHP} = \int_{\text{D26}}^{0} c_P\, \rho_{T,S}(T(z) - 26℃)dz \tag{4}$$

where c_P is the specific heat capacity of the seawater (=4200 J kg^{-1} $°C^{-1}$), and T(z) denotes the upper-ocean temperature structure that includes the SST.

For this product, density (ρ) is calculated at every depth (z) using a forth order polynomial dependent on temperature (T) and salinity (S = 35 psu).

Data availability

The International Best Track Archive for Climate Stewardship (IBTrACS) dataset, provided by the National Centers for Environmental Information (NCEI), is available from https://www.ncei.noaa.gov/products/international-best-track-archive. The sea surface temperature (SST) data used in this study were obtained from the ERA5 dataset, provided by the Copernicus Climate Change Service (C3S), and are publicly available at https://cds.climate.copernicus.eu/cdsapp#!/dataset/reanalysis-era5-single-levels?tab=form. The analysis of the environmental parameters in Table 1 and Fig. 9 was carried out for the period 2013–2022. TCHP, D26, and MLD data were obtained from the NOAA's Operational Satellite Ocean Heat Content Suite, available at the National Centers for Environmental Information (NCEI) website (https://www.ncei.noaa.gov/products/satellite-ocean-heat-content-suite). LHF data were sourced from the ERA5 hourly data on single levels, accessible via the Copernicus Climate Data Store (https://cds.climate.copernicus.eu/cdsapp#!/dataset/reanalysis-era5-single-levels?tab=form). Data for VWS were calculated based on *u* and *v* component wind speeds at 200- and 850 hPa pressure levels, obtained from ERA5 hourly data on pressure levels. This dataset is also available on the Copernicus Climate Data Store (https://cds.climate.copernicus.eu/cdsapp#!/dataset/reanalysis-era5-pressure-levels?tab=form). Other data that used for creating the plots are freely available in the data folder of our GitHub pages (see the "Code availability" section for links).

Code availability

All codes developed for conducting analyses, generating results, and creating plots are available on our GitHub pages: https://github.com/sradfar/GoM_ProbRI-MHW and https://github.com/CHL-UA.

Received: 3 November 2023; Accepted: 23 July 2024;
Published online: 09 August 2024

References

1. Bucci, L., Alaka, L., Hagen, A., Delgado, S. & Beven, J. *Hurricane Ian report (AL092022)* (National Hurricane Center, 2023).
2. Dzwonkowski, B. et al. Cascading weather events amplify the coastal thermal conditions prior to the shelf transit of Hurricane Sally (2020). *J. Geophys. Res. Oceans* **126**, e2021JC017957 (2021).
3. Trabing, B. C. & Bell, M. M. Understanding error distributions of hurricane intensity forecasts during rapid intensity changes. *Weather Forecast.* **35**, 2219–2234 (2020).
4. Lee, C.-Y., Tippett, M. K., Sobel, A. H. & Camargo, S. J. Rapid intensification and the bimodal distribution of tropical cyclone intensity. *Nat. Commun.* **7**, 10625 (2016).
5. Emanuel, K. Will global warming make hurricane forecasting more difficult? *Bull. Am. Meteorol. Soc.* **98**, 495–501 (2017).
6. Hong, J. & Wu, Q. Modulation of global sea surface temperature on tropical cyclone rapid intensification frequency. *Environ. Res. Commun.* **3**, 041001 (2021).
7. Pielke, R. A. *The Hurricane* (Routledge, 2013).
8. Cione, J. J. The relative roles of the ocean and atmosphere as revealed by buoy air–sea observations in hurricanes. *Mon. Weather Rev.* **143**, 904–913 (2015).
9. Cione, J. J. & Uhlhorn, E. W. Sea surface temperature variability in hurricanes: implications with respect to intensity change. *Mon. Weather Rev.* **131**, 1783–1796 (2003).
10. Zscheischler, J. et al. A typology of compound weather and climate events. *Nat. Rev. Earth Environ.* **1**, 333–347 (2020).
11. Dzwonkowski, B. et al. Compounding impact of severe weather events fuels marine heatwave in the coastal ocean. *Nat. Commun.* **11**, 4623 (2020).
12. Mawren, D., Hermes, J. & Reason, C. Marine heat waves and tropical cyclones-two devastating types of coastal hazard in South-Eastern Africa. *Estuar. Coast. Shelf Sci.* **277**, 108056 (2022).
13. Rathore, S. et al. Interactions between a marine heatwave and Tropical Cyclone Amphan in the Bay of Bengal in 2020. *Front. Clim.* **4**, 861477 (2022).
14. Le Hénaff, M. et al. The role of the Gulf of Mexico ocean conditions in the intensification of Hurricane Michael (2018). *J. Geophys. Res. Oceans* **126**, e2020JC016969 (2021).
15. Choi, H.-Y., Park, M.-S., Kim, H.-S. & Lee, S. Marine heatwave events strengthen the intensity of tropical cyclones. *Commun. Earth Environ.* **5**, 69 (2024).
16. Narayanan, A., Balaguru, K., Xu, W. & Leung, L. R. A new method for predicting hurricane rapid intensification based on co-occurring environmental parameters. *Nat. Hazards* **120**, 881–899 (2024).
17. Rozoff, C. M., Velden, C. S., Kaplan, J., Kossin, J. P. & Wimmers, A. J. Improvements in the probabilistic prediction of tropical cyclone rapid intensification with passive microwave observations. *Weather Forecast.* **30**, 1016–1038 (2015).
18. Balaguru, K. et al. Pronounced impact of salinity on rapidly intensifying tropical cyclones. *Bull. Am. Meteorol. Soc.* **101**, E1497–E1511 (2020).
19. Gao, S., Zhai, S., Chiu, L. S. & Xia, D. Satellite air–sea enthalpy flux and intensity change of tropical cyclones over the western North Pacific. *J. Appl. Meteorol. Climatol.* **55**, 425–444 (2016).
20. Drennan, W. M., Zhang, J. A., French, J. R., McCormick, C. & Black, P. G. Turbulent fluxes in the hurricane boundary layer. Part II: latent heat flux. *J. Atmos. Sci.* **64**, 1103–1115 (2007).
21. Zhang, Z., Zhang, W., Zhao, W. & Zhao, C. Radial distributions of sea surface temperature and their impacts on the rapid intensification of Typhoon Hato (2017). *Atmosphere* **11**, 128 (2020).
22. Gramer, L. J., Zhang, J. A., Alaka, G., Hazelton, A. & Gopalakrishnan, S. Coastal downwelling intensifies landfalling hurricanes. *Geophys. Res. Lett.* **49**, e2021GL096630 (2022).
23. Perrie, W. et al. Sea spray impacts on intensifying midlatitude cyclones. *J. Atmos. Sci.* **62**, 1867–1883 (2005).
24. Oliver, E. C., Perkins-Kirkpatrick, S. E., Holbrook, N. & Bindoff, N. Anthropogenic and natural influences on record 2016 marine heat waves. *Bull. Am. Meteorol. Soc.* **99**, 44–48 (2018).
25. Holbrook, N. J. et al. A global assessment of marine heatwaves and their drivers. *Nat. Commun.* **10**, 2624 (2019).
26. Sen Gupta, A. et al. Drivers and impacts of the most extreme marine heatwave events. *Sci. Rep.* **10**, 19359 (2020).
27. Elzahaby, Y. & Schaeffer, A. Observational insight into the subsurface anomalies of marine heatwaves. *Front. Mar. Sci.* **6**, 745 (2019).
28. Jangir, B., Swain, D. & Ghose, S. Influence of eddies and tropical cyclone heat potential on intensity changes of tropical cyclones in the North Indian Ocean. *Adv. Space Res.* **68**, 773–786 (2021).
29. Balaguru, K. et al. Ocean barrier layers' effect on tropical cyclone intensification. *Proc. Natl Acad. Sci.* **109**, 14343–14347 (2012).
30. Wang, Y., Tan, Z.-M. & Li, Y. Some refinements to the most recent simple time-dependent theory of tropical cyclone intensification and sensitivity. *J. Atmos. Sci.* **80**, 321–335 (2023).
31. Xu, J., Wang, Y. & Tan, Z.-M. The relationship between sea surface temperature and maximum intensification rate of tropical cyclones in the North Atlantic. *J. Atmos. Sci.* **73**, 4979–4988 (2016).
32. Knutson, T. R. et al. Global projections of intense tropical cyclone activity for the late twenty-first century from dynamical downscaling of CMIP5/RCP4. 5 scenarios. *J. Clim.* **28**, 7203–7224 (2015).
33. Frölicher, T. L., Fischer, E. M. & Gruber, N. Marine heatwaves under global warming. *Nature* **560**, 360–364 (2018).
34. NOAA National Centers for Environmental Information. Continental United States hurricane strikes 1950-2022 https://www.ncei.noaa.gov/pub/data/images/US_Hurricane_Strikes/ (2023).

35. NOAA. The deadliest, costliest and most intense U.S. Tropical Cyclones https://www.ncei.noaa.gov/access/billions/dcmi.pdf (2024).
36. Knapp, K. R. D. et al. *International Best Track Archive for Climate Stewardship (IBTrACS) Project, Version 4* (NOAA National Centers for Environmental Information, 2018).
37. Jaimes, B., Shay, L. K. & Uhlhorn, E. W. Enthalpy and momentum fluxes during Hurricane Earl relative to underlying ocean features. *Mon. Weather Rev.* **143**, 111–131 (2015).
38. Jaimes, B., Shay, L. K. & Brewster, J. K. Observed air-sea interactions in tropical cyclone Isaac over Loop Current mesoscale eddy features. *Dyn. Atmos. Oceans* **76**, 306–324 (2016).
39. Hobday, A. J. et al. A hierarchical approach to defining marine heatwaves. *Prog. Oceanogr.* **141**, 227–238 (2016).
40. Feng, Y.-T. et al. Marine heatwaves in the Gulf of Mexico 1983–2021: statistics, recent intensifications, and threats on coral reefs. *Adv. Clim. Change Res.* **14**, 560–572 (2023).
41. Weisberg, R. H. & Liu, Y. On the loop current penetration into the Gulf of Mexico. *J. Geophys. Res. Oceans* **122**, 9679–9694 (2017).
42. Smith, K. E. et al. Biological impacts of marine heatwaves. *Annu. Rev. Mar. Sci.* **15**, 119–145 (2023).
43. Ratnarajah, L. et al. Monitoring and modelling marine zooplankton in a changing climate. *Nat. Commun.* **14**, 564 (2023).
44. Zhang, X., Hegerl, G., Zwiers, F. W. & Kenyon, J. Avoiding inhomogeneity in percentile-based indices of temperature extremes. *J. Clim.* **18**, 1641–1651 (2005).
45. Zhang, X., Zheng, F., Zhu, J. & Chen, X. Observed frequent occurrences of marine heatwaves in most ocean regions during the last two decades. *Adv. Atmos. Sci.* **39**, 1579–1587 (2022).
46. Mainelli, M., DeMaria, M., Shay, L. K. & Goni, G. Application of oceanic heat content estimation to operational forecasting of recent Atlantic category 5 hurricanes. *Weather Forecast.* **23**, 3–16 (2008).
47. Domingues, C. M. et al. Improved estimates of upper-ocean warming and multi-decadal sea-level rise. *Nature* **453**, 1090–1093 (2008).
48. Ishii, M. & Kimoto, M. Reevaluation of historical ocean heat content variations with time-varying XBT and MBT depth bias corrections. *J. Oceanogr.* **65**, 287–299 (2009).
49. Levitus, S. et al. Global ocean heat content 1955–2008 in light of recently revealed instrumentation problems. *Geophys. Res. Lett.* **36**, L07608 (2009).
50. Hayashi, M., Shiogama, H., Emori, S., Ogura, T. & Hirota, N. The northwestern Pacific warming record in August 2020 occurred under anthropogenic forcing. *Geophys. Res. Lett.* **48**, e2020GL090956 (2021).
51. Palmer, M. D. et al. Ocean heat content variability and change in an ensemble of ocean reanalyses. *Clim. Dyn.* **49**, 909–930 (2017).
52. Kaplan, J. & DeMaria, M. Large-scale characteristics of rapidly intensifying tropical cyclones in the North Atlantic basin. *Weather Forecast.* **18**, 1093–1108 (2003).
53. Ray, A., Das, S. & Sil, S. Role of anomalous ocean warming on the intensification of pre-monsoon tropical cyclones over the Northern Bay of Bengal. *J. Geophys. Res. Oceans* **129**, e2023JC020527 (2024).
54. Paterson, L. A., Hanstrum, B. N., Davidson, N. E. & Weber, H. C. Influence of environmental vertical wind shear on the intensity of hurricane-strength tropical cyclones in the Australian region. *Mon. Weather Rev.* **133**, 3644–3660 (2005).
55. Ryglicki, D. R., Cossuth, J. H., Hodyss, D. & Doyle, J. D. The unexpected rapid intensification of tropical cyclones in moderate vertical wind shear. Part I: overview and observations. *Mon. Weather Rev.* **146**, 3773–3800 (2018).
56. Trenberth, K. E., Cheng, L., Jacobs, P., Zhang, Y. & Fasullo, J. Hurricane Harvey links to ocean heat content and climate change adaptation. *Earths Future* **6**, 730–744 (2018).
57. Trenberth, K. E. & Fasullo, J. Water and energy budgets of hurricanes and implications for climate change. *J. Geophys. Res. Atmos.* **112**, D23107 (2007).
58. Dzwonkowski, B. et al. Hurricane Sally (2020) shifts the ocean thermal structure across the inner core during rapid intensification over the shelf. *J. Phys. Oceanogr.* **52**, 2841–2852 (2022).
59. Klotzbach, P. J. El Niño–Southern Oscillation's impact on Atlantic basin hurricanes and US landfalls. *J. Clim.* **24**, 1252–1263 (2011).
60. Klotzbach, P., Bell, M. & DesRosiers, A. *Summary of 2023 Atlantic Tropical Cyclone Activity and Verification of Authors' Seasonal and Two-week Forecasts* (Department of Atmospheric Science, Colorado State University, 2023).
61. Leijnse, T. W. B., Giardino, A., Nederhoff, K. & Caires, S. Generating reliable estimates of tropical-cyclone-induced coastal hazards along the Bay of Bengal for current and future climates using synthetic tracks. *Nat. Hazards Earth Syst. Sci.* **22**, 1863–1891 (2022).
62. Nederhoff, K. et al. Simulating synthetic tropical cyclone tracks for statistically reliable wind and pressure estimations. *Nat. Hazards Earth Syst. Sci.* **21**, 861–878 (2021).
63. Xi, D., Lin, N. & Gori, A. Increasing sequential tropical cyclone hazards along the US East and Gulf coasts. *Nat. Clim. Change* **13**, 258–265 (2023).
64. Marsooli, R., Lin, N., Emanuel, K. & Feng, K. Climate change exacerbates hurricane flood hazards along US Atlantic and Gulf Coasts in spatially varying patterns. *Nat. Commun.* **10**, 3785 (2019).
65. Li, Y. et al. Leveraging LSTM for rapid intensifications prediction of tropical cyclones. *ISPRS Ann. Photogramm. Remote Sens. Spat. Inf. Sci.* **4**, 101–105 (2017).
66. Yang, Q., Lee, C.-Y. & Tippett, M. K. A long short-term memory model for global rapid intensification prediction. *Weather Forecast.* **35**, 1203–1220 (2020).
67. Jacox, M. G. et al. Global seasonal forecasts of marine heatwaves. *Nature* **604**, 486–490 (2022).
68. Lawman, A., Dee, S., DeLong, K. & Correa, A. Rates of future climate change in the Gulf of Mexico and the Caribbean Sea: implications for coral reef ecosystems. *J. Geophys. Res. Biogeosci.* **127**, e2022JG006999 (2022).
69. Oliver, E. C. et al. Longer and more frequent marine heatwaves over the past century. *Nat. Commun.* **9**, 1–12 (2018).
70. Cheng, Y. et al. A quantitative analysis of marine heatwaves in response to rising sea surface temperature. *Sci. Total Environ.* **881**, 163396 (2023).
71. Huang, B. et al. Improvements of the daily optimum interpolation sea surface temperature (DOISST) version 2.1. *J. Clim.* **34**, 2923–2939 (2021).
72. Hersbach, H. et al. The ERA5 global reanalysis. *Q. J. R. Meteorol. Soc.* **146**, 1999–2049 (2020).
73. Yao, L., Lu, J., Xia, X., Jing, W. & Liu, Y. Evaluation of the ERA5 sea surface temperature around the Pacific and the Atlantic. *IEEE Access* **9**, 12067–12073 (2021).
74. Radfar, S., Shafieefar, M., Akbari, H., Galiatsatou, P. A. & Mazyak, A. R. Design of a rubble mound breakwater under the combined effect of wave heights and water levels, under present and future climate conditions. *Appl. Ocean Res.* **112**, 102711 (2021).
75. Kossin, J. P., Knapp, K. R., Olander, T. L. & Velden, C. S. Global increase in major tropical cyclone exceedance probability over the past four decades. *Proc. Natl Acad. Sci.* **117**, 11975–11980 (2020).
76. Oliver, E. C. et al. Projected marine heatwaves in the 21st century and the potential for ecological impact. *Front. Mar. Sci.* **6**, 734 (2019).
77. Schlegel, R. W. & Smit, A. J. heatwaveR: a central algorithm for the detection of heatwaves and cold-spells. *J. Open Source Softw.* **3**, 821 (2018).
78. Vecchi, G. A. & Soden, B. J. Effect of remote sea surface temperature change on tropical cyclone potential intensity. *Nature* **450**, 1066–1070 (2007).

79. Ramsay, H. A. & Sobel, A. H. Effects of relative and absolute sea surface temperature on tropical cyclone potential intensity using a single-column model. *J. Clim.* **24**, 183–193 (2011).
80. Von Kietzell, A., Schurer, A. & Hegerl, G. C. Marine heatwaves in global sea surface temperature records since 1850. *Environ. Res. Lett.* **17**, 084027 (2022).
81. Oguejiofor, C. N., Wainwright, C. E., Rudzin, J. E. & Richter, D. H. Onset of tropical cyclone rapid intensification: evaluating the response to length scales of sea surface temperature anomalies. *J. Atmos. Sci.* **80**, 1971–1994 (2023).
82. Kafatos, M. et al. Role of anomalous warm gulf waters in the intensification of Hurricane Katrina. *Geophys. Res. Lett.* **33**, L17802 (2006).
83. Miyamoto, Y. & Takemi, T. An effective radius of the sea surface enthalpy flux for the maintenance of a tropical cyclone. *Atmos. Sci. Lett.* **11**, 278–282 (2010).
84. Zhang, J. A. et al. Observations of infrared sea surface temperature and air–sea interaction in Hurricane Edouard (2014) using GPS dropsondes. *J. Atmos. Ocean. Technol.* **34**, 1333–1349 (2017).
85. Chan, K. T. & Chan, J. C. The outer-core wind structure of tropical cyclones. *J. Meteorol. Soc. Jpn. Ser. II* **96**, 297–315 (2018).
86. Wang, Y. & Xu, J. Energy production, frictional dissipation, and maximum intensity of a numerically simulated tropical cyclone. *J. Atmos. Sci.* **67**, 97–116 (2010).
87. Qiu, Z., Qiao, F., Jang, C. J., Zhang, L. & Song, Z. Evaluation and projection of global marine heatwaves based on CMIP6 models. *Deep Sea Res. Part II Top. Stud. Oceanogr.* **194**, 104998 (2021).
88. Jacox, M. G., Alexander, M. A., Bograd, S. J. & Scott, J. D. Thermal displacement by marine heatwaves. *Nature* **584**, 82–86 (2020).
89. Weatherford, C. L. & Gray, W. M. Typhoon structure as revealed by aircraft reconnaissance. Part I: data analysis and climatology. *Mon. Weather Rev.* **116**, 1032–1043 (1988).
90. Tripathy, K. P., Mukherjee, S., Mishra, A. K., Mann, M. E. & Williams, A. P. Climate change will accelerate the high-end risk of compound drought and heatwave events. *Proc. Natl Acad. Sci.* **120**, e2219825120 (2023).
91. Maturi, E. M., Shay, L. N., Donahue, D. R. & Byrne, D. A. NOAA's operational satellite ocean heat content products. *J. Oper. Oceanogr.* **17**, 1–10 (2022).

Acknowledgements

We would like to thank the reviewers for their helpful comments during the review process, which helped us improve the quality of this article. Funding was awarded to Cooperative Institute for Research to Operations in Hydrology (CIROH) through the NOAA Cooperative Agreement with The University of Alabama (NA22NWS4320003). Partial support was also provided by NSF award # 2223893.

Author contributions

S.R. and H.Mof. conceptualized the study and designed the framework. S.R. collected the data and implemented the analysis. H.Mof. supervised the work. S.R. wrote the first draft of the manuscript. H.Mof. and H.Mor. provided comments, edited the manuscript, and secured funding.

Competing interests

The authors declare no competing interests.

Additional information

Supplementary information The online version contains supplementary material available at https://doi.org/10.1038/s43247-024-01578-2.

Correspondence and requests for materials should be addressed to Soheil Radfar.

Peer review information *Communications Earth and Environment* thanks Vineet Kumar Singh, Albertus Smit and the other, anonymous, reviewer(s) for their contribution to the peer review of this work. Primary Handling Editor: Heike Langenberg. A peer review file is available.